Journal of Alloys and Compounds 509 (2011) 2639–2644

Contents lists available at ScienceDirect

Journal of Alloys and Compounds

journal homepage: www.elsevier.com/locate/jallcom

First-principles study of nickel-silicides ordered phases

Damien Connétable[a,*], Olivier Thomas[b,c]

[a] CIRIMAT (UMR 5085), ENSIACET CNRS-INPT-UPS, 4, allée Emile Monso, BP 44362, F-31030 TOULOUSE Cedex 4, France
[b] Aix-Marseille Université, IM2NP, France
[c] CNRS, IM2NP (UMR 6242), Faculté des Sciences et Techniques, Campus de St Jérome, F-13397 Marseille Cedex, France

ARTICLE INFO

Article history:
Received 2 August 2010
Received in revised form 17 October 2010
Accepted 22 October 2010
Available online 4 November 2010

Keywords:
Nickel
Silicon
Phase diagram
Ordered alloys
DFT

ABSTRACT

We present a study of nickel-silicides ordered alloys by means of first-principles calculations. Emphasis was put on the phases (low and high temperatures) identified in the binary phase diagram, namely: Ni_3Si-β_1, -β_2, and -β_3, $Ni_{31}Si_{12}$-γ, Ni_2Si-δ, -θ, Ni_3Si_2-ε, NiSi-MnP and $NiSi_2$-α. In addition, some common structures are computed for information: $L1_2$, $D0_3$ and $D0_{22}$. The simulations reproduce with a high accuracy lattice parameters and formation energies of main experimental structures, except for β_2 and β_3. Our results clarify the crystallographic nature of the γ structure, and the comparison of experimental Raman spectra and vibrational calculations will help experimentalists to identify without ambiguity $NiSi_3$ structures.

1. Introduction

Nickel silicides are used for contacts in complementary metal oxide semiconductor (CMOS) devices to reduce the resistance between the Si substrates and electrodes, and also as gate electrodes to improve gate sheet resistance and poly-depletion. Knowledge about the structure and properties of nickel silicides is therefore critical to be able to control and understand their formation during reactive diffusion at the nanometer scale. Recent works suggest the stabilization of new phases in the ultra-thin film regime. Such findings clearly spurs in-depth work on the stability of nickel-silicon phases.

Ni–Si phase diagram has been assessed by Lindholm [1], and Tokunaga [2], either from experimental data, or from DFT calculations.

The aim of this paper is to revisit nickel-silicide systems by means of first-principles methods. Emphasis has been put on phases present in the phase diagram, as well as some metastable systems. Their formation energies and ground properties are discussed according to the experimental measurements and assessed values available in literature. The phase diagram described by Massalski [3] (see Fig. 1) is composed of 13 phases: three polymorphic Ni_3Si structures (β_1, β_2 and β_3 the low and high temperatures phases respectively), $Ni_{31}Si_{12}$ (γ), two polymorphic Ni_2Si structures (δ = C23 and θ = $B8_2$), Ni_3Si_2 = ε, NiSi (MnP) and $NiSi_2$ (α = CaF_2). We do not discuss about $NiSi_2$-β and Ni_3Si_2-ε' because of absence of experimental data.

Some complementary structures are presented: Ni_2Si/$NiSi_3$-$D0_3$, -$D0_{22}$, the Ni_5Si_2 phase ($D8_h$) used by Tokunaga [2] to describe γ, Ni_2Si (C37 prototype), $NiSi_2$ ($CaCl_2$ = C35), and NiSi-$L1_0$.

2. Computational details

Ni–Si alloys have been computed by means of the density functional theory (DFT) (Vienna Ab initio Simulation Package, VASP [4]). The Perdew–Burke–Ernzerhof [5] (PBE) generalized gradient approximation of the exchange and correlation functional within its spin-polarized version and projected Augmented Waves pseudo-potentials [6] (PAW) have been used in this study. We have employed a 400 eV energy cut-off, and dense mesh grids (around 5000 k-points atom/cell) to optimize unit cells. For example, it corresponds to $17 \times 17 \times 17$ k-mesh grid for cfc-Ni or Si-diamond, and $4 \times 4 \times 8$ for Ni_3Si_2 (80 atoms in the unit cell). To compute formation energies, finest grids (around 10,000 k-points atom/cell) and higher energies cut-off (500 eV) have been adopted, this provides a sufficient convergence (around 1 meV/atom).

3. Results and discussion

3.1. Reference states (Ni-A1 and Si-A4)

Ni-fcc ferromagnetic and silicon diamond phases have been used as references states to calculate formation energies of the structures at intermediate compositions. Both pseudo-potentials

* Corresponding author.
E-mail address: damien.connetable@ensiacet.fr (D. Connétable).

0925-8388/$ – see front matter © 2010 Elsevier B.V. All rights reserved.
doi:10.1016/j.jallcom.2010.10.118

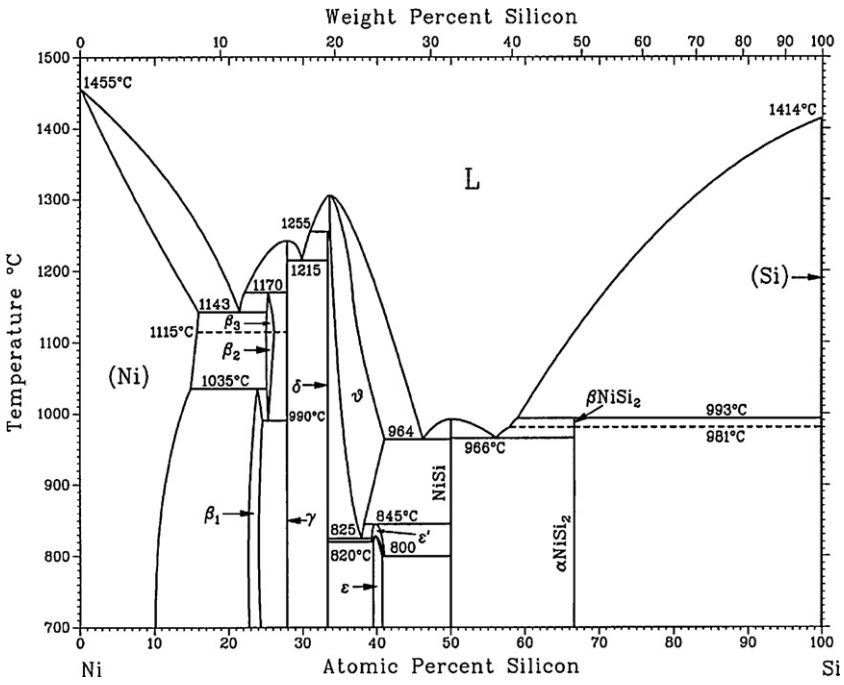

Fig. 1. Ni–Si phase diagram from Massalski [3].

used reproduce with a great accuracy lattice parameters, and elastic properties (see results presented in Ref. [7]). The cohesive energies are found in agreement with literature: 4.83 eV and 4.57 eV. These values are in good agreement with experimental data 4.44 eV and 4.63 eV for nickel and silicon respectively [8]. In the case of nickel, it has been shown that the DFT cohesive energy is overestimated by 0.1–0.3 eV (see the discussion Ref. [9]).

3.2. $\beta_{1,2,3}$-Ni_3Si

At 25% in composition in silicon, three polymorphic phases have been identified, labeled β_1, β_2, and β_3.

β_1 is the low temperature phase. It is a $L1_2$-type structure (2 2 1 space group), where Si and Ni are located in *1a*, and *3c* Wyckoff positions respectively. The lattice parameter is 3.506 Å [10,11]. Simulations reproduce with a great accuracy this lattice parameter (discrepancy <1%, see Table 1). One finds in the literature only one value for its formation energy (Tokunaga 2003 [2]). We notice a small, but significant, disagreement between our calculated value and the value given by Tokunaga. In their paper, they do not indicate the magnetic state used for nickel-fcc. We have evaluated the difference between the formation energy of nickel without magnetism and with magnetism: $\Delta E = E(\mathrm{Ni_{mag}}) - E(\mathrm{Ni_{non\,mag}}) \simeq 50 - 60$ meV/atom. ΔE corresponds well to the difference between our value and the one from Tokunaga. We conclude that they have neglected the magnetism in their simulations, which induces a small shift between the formation energies presented here and theirs.

Whereas the β_1 phase is well described in the literature, the crystallographic nature of the two other polymorphic β structures do not remain clear. For Ram [12], β_2 and β_3 are squaring with two phases with the same monoclinic structure, with Cu_3Au prototype ($D0_{15}$ No. 12, *4g*, *4i*, *8j* for Si and Ni positions respectively). The lattice parameters of these two structures are found slightly different, and they concluded that these two phases may exhibit probably "a different order". On its side, Bhan and Kudielka [13] have identified two structures at high temperatures but with the $Pm\,\bar{3}m$ group symmetry (No. 221, CsCl prototype). Finally, Leballi and Hamar-Thibault [11] have identified two other structures with the same Pnma group symmetry (No. 62, orthorhombic Fe_3C prototype, where Si are located in *4c* position and Ni in *8d*). The only crosscheck has been made by Song and Jin [14], who have recently synthesized β_3-Ni_3Si nanowires with a monoclinic Bravais lattice. This last results seem thus to confirm Ram's data.

To clarify experimental results, we have computed five structures with different point groups: $D0_{15}$, $D0_{11}$, $P2_12_12$, $D0_3$ and $D0_{22}$. Results are summarized in the Table 1. Any simulated lattice parameters correspond to any experimental data. For example, in the case of $D0_{11}$ or $D0_{15}$ structures, the discrepancy with experimental observations is strong. Intrinsic defects, temperature or disordered structure – these phases have been identified at high temperature – could explain the discrepancy between the theory and experimental observations.

3.3. γ: $Ni_{31}Si_{12}$ or Ni_5Si_2

At an intermediate composition (around 28 at.% Si), one finds one crystallographic structure labeled γ. The symmetry, reported by Franck [15], is hexagonal (hP14) with the $Ni_{31}Si_{12}$ composition (space group No. 150). We have reported in the Table 2 their Wyckoff atomic positions. It is a complex structure with 43 atoms per unit cell (see Fig. 2).

For Leballi and Hamar-Thibault [11], γ should have a hexagonal symmetry but with an other space group (No. 194) and an other composition: Ni_5Si_2, composition closed to the one proposed by Franck. Nickel are then put in *2a*, *2b*, *4f*, and silicon in *4f* positions.

To work out the disagreement, we have studied both structures and compared DFT lattice parameters and formation energies with those published in the literature [2,16]. We find that the optimized lattice parameters are in agreement with experimental data associated with the structure proposed by Franck (less 1% of discrepancy). At 0 K, $Ni_{31}Si_{12}$ is moreover more stable than Ni_5Si_2, and its calculated formation energy agrees well with the assessed value [2,16]. All these results indicate that γ should be $Ni_{31}Si_{12}$.

Table 1
Optimized and experimental lattice parameters (in Å), formation energies E_0 (in meV/atom), and total magnetic moment (in Bohr's magneton) of the Ni–Si alloys. PS = Pearson Strukturbericht, Ass. = Assessed values.

System	Name	PS	symbol		a_0	b_0 (Å)	c_0	β (degree)	E_0 (meV/atom)	μ_B
Ni		Expt. [8]	cF4 (223)	A1	3.519	–	–	–	–	0.62
		PAW			3.520	–	–	–	0	0.63
Ni_3Si	β_1	Expt. [10]	cP4 (221)	$L1_2$	3.506		–	–	−416[1]/−510[2]	–
		PAW			3.512	–	–	–	−463	0.00
	β_2	Expt. [12]	mC16 (12)	$D0_{15}$	6.972	6.254	7.656	87.75	–	–
		PAW			4.729	7.555	10.223	–	−175	0.00
	β_3	Expt. [12,14]	mC16 (12)	$D0_{15}$	7.047	6.264	7.663	87.14	–	–
		PAW	oP16 (18)	$P2_12_12$	5.374	7.949	4.096	117.39	−324	0.00
	β_3	Expt. [11]	oP16 (62)	$D0_{11}$	5.50	6.50	4.35	–	−379[1]	–
		PAW			4.964	7.022	4.964	–	−463	0.00
		PAW	cF16 (225)	$D0_3$	5.586	–	–	–	−385	0.00
		Ass. [2]	tI8 (139)	$D0_{22}$	–	–	–	–	−460	–
		PAW			3.586	–	3.380	–	−419	0.00
$Ni_{31}Si_{12}$	γ	Expt. [15]	hP14 (150)		6.671	–	12.288	–	–	–
		PAW			6.668	–	12.319	–	−499	0.00
Ni_5Si_2		Ass. [16,2]	hP14 (194)	$D8_h$	–	–	–	–	−438/−451	–
		PAW			3.950	–	11.909	–	−153	0.00
Ni_2Si	δ	Expt. [17]	oP12 (62)	C23	5.009	3.732	7.066	–	−486[16]	–
		PAW			5.079	3.700	7.069	–	−556	0.00
	θ	Expt. [18]	hP6 (182)	$B8_2$	3.805	–	4.890	–	−412[1]	–
		PAW			3.916	–	4.992	–	−509	0.00
Ni_3Si_2	ε	Expt. [19]	oP80 (36)		12.229	10.805	6.924	–	−472[16]	–
		PAW			12.299	10.798	6.924	–	−526	0.00
NiSi		Expt. [20]	oP8 (62)	P31	5.177	3.325	5.616	–	−447[16]	–
		PAW			5.165	3.378	5.621	–	−503	0.00
		Ass. [2]	tP2 (123)	$L1_0$	–	–	–	–	−169	–
		PAW			3.718	–	3.310	–	−290	0.00
	α	Expt. [21]	cF12 (225)	C1	5.43	–	–	–	−303[16]/−352[1]	–
$NiSi_2$		PAW			5.470	–	–	–	−348	0.00
		PAW	oP6 (58)	C35	5.430	4.947	3.450	–	+4	0.00
$NiSi_3$		Ass. [2]	cP4 (221)	$L1_2$	–	–	–	–	+214	–
		PAW			3.748	–	–	–	+237	0.00
		PAW	cF16 (225)	$D0_3$	5.984	–	–	–	+286	0.00
		Ass. [2]	tI8 (139)	$D0_{22}$	–	–	–	–	+177	–
		PAW			3.824	–	3.562	–	+200	0.00
Si		Expt. [8]	cF8 (227)	A4	5.43	–	–	–	–	0.00
		PAW			5.468	–	–	–	0	0.00
		Ass[2]	cF4 (223)	A1	–	–	–	–	+553	0.00
		PAW			3.865	–	–	–	+542	0.00

3.4. δ- and θ-Ni_2Si

Two allotropic forms are reported for Ni_2Si (Toman [18], and Föll et al. [22]): labeled δ and θ, the low and high temperature structures respectively (see phase diagram from Richter et al. [23], Fig. 3). The more thermodynamically stable phase at low temperature is the δ structure.

Table 2
Wyckoff atomic positions of $Ni_{31}Si_{12}$ (γ) hexagonal phase (space group P321) from Ref. [15].

Wyckoff position	x	y	z	x	y	z
	Ni			Si		
1b	0	0	1/2			
2c	0	0	0.095	0	0	0.28
2d	1/3	2/3	0.071	1/3	2/3	0.27
2d	1/3	2/3	0.566	1/3	2/3	0.77
6g	0.41	0.07	0.096			
6g	0.66	0.96	0.198			
6g	0.35	0.03	0.306			
6g	0.62	0.93	0.404			
3e				0.682	0	0
3f				0.349	0	1/2

δ-Ni_2Si is an orthorhombic structure with the space group No. 62 (oP12). All atoms are located in *4c* positions (see Fig. 4). We reproduce experimental lattice parameters, and the formation energy is in the same range as the assessed value proposed by Oelson and Samson-Himmelstjerna [16].

The second structure – θ-Ni_2Si – has a hexagonal symmetry, with the space group No. 182. Nickel and silicon are located in *2a, 2d*, and *2c* sites respectively. It is a high temperature phase, only one measurement has been reported (measured by Toman [18]). The optimized lattice parameters are found slightly greater than the experimental ones (around 2–3%). From an energetic point of view, we find also that θ is less stable than δ.

3.5. ε-Ni_3Si_2

The Ni_3Si_2-ε phase has been described by Pilström [24]. This orthorhombic phase is a complex structure with 80 atoms per unit cell (space group No. 36, Fig. 5). We report the atomic position in the Table 3. As for previous systems, first-principles calculations (see Table 1) yields, with a good accuracy, experimental lattice parameters.

Table 3
Wyckoff atomic positions of Ni_3Si_2 (ε) orthorhombic structure (space group No. 36, $Cmc2_1$) from Ref. [24].

Wyckoff position	x	y	z	x	y	z
	Ni			Si		
4a	0	0	0	0	0.1570	0.7120
4a	0	0.2345	0.0240	0	0.4090	0.2180
4a	0	0.2330	0.4000			
4a	0	0.3814	0.7140			
8b	0.1732	0.1177	0.5180	0.1520	0.3440	0.5060
8b	0.1723	0.1189	0.9000	0.1510	0.3430	0.9200
8b	0.1972	0.2467	0.2170	0.1200	0.0590	0.2140
8b	0.1824	0.4975	0.2250			

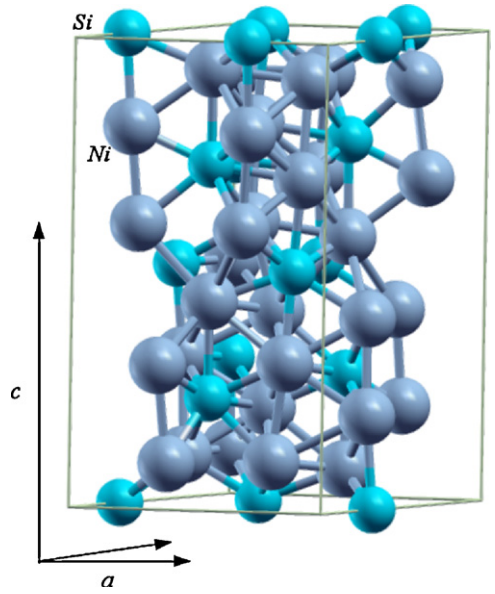

Fig. 2. Symbolic representation of $Ni_{31}Si_{12}$. In gray and blue we have represented nickel and silicon atoms respectively. (For interpretation of the references to color in this figure legend, the reader is referred to the web version of the article.)

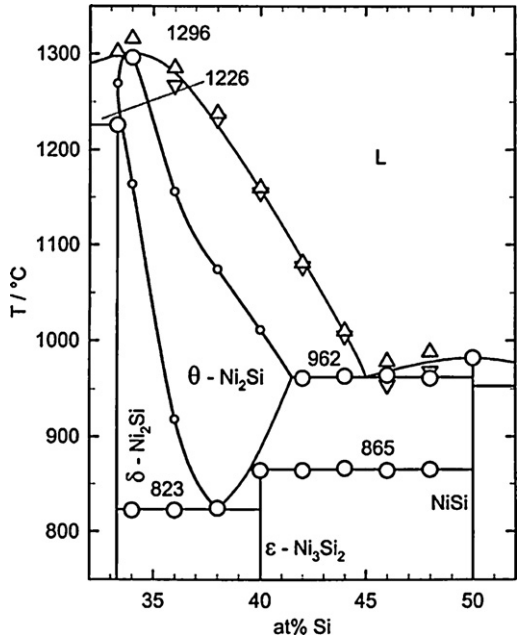

Fig. 4. Phase diagram at 33–66% in silicon [23].

3.6. MnP-NiSi

The MnP-NiSi structure (oP8, space group No. 62) has been already characterized in a previous work [7]. Lattice parameters have been found in agreement with experimental data, and we have found that the formation energy is slightly smaller than the value used by Lindholm and Sundman [1] in his assessment.

3.7. α-$NiSi_2$

Up to 50% in silicon, only one phase at low temperature has been identified: $NiSi_2$ with the cF12 crystallographic group (CaF_2 prototype). The unit cell is composed of three atoms per unit cell. The optimized lattice parameter is found in agreement with the experimental value [21] (<1%), its formation energy is found greater than other Ni–Si system.

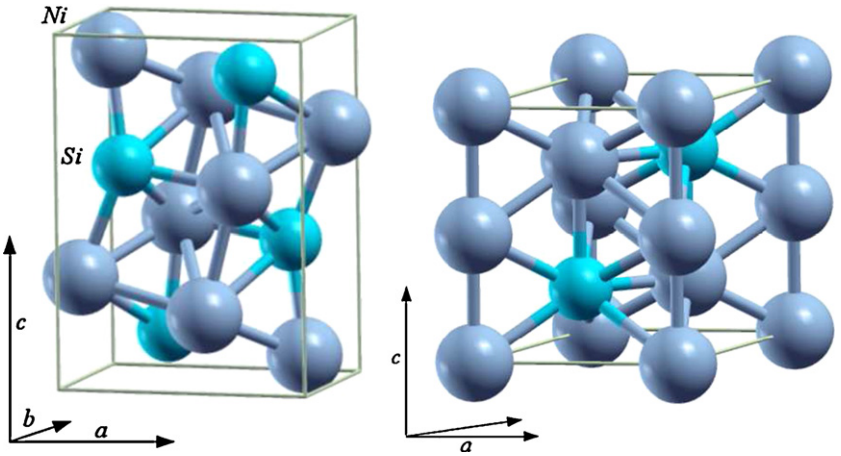

Fig. 3. Symbolic representation of δ-(left) and θ-Ni_2Si (right).

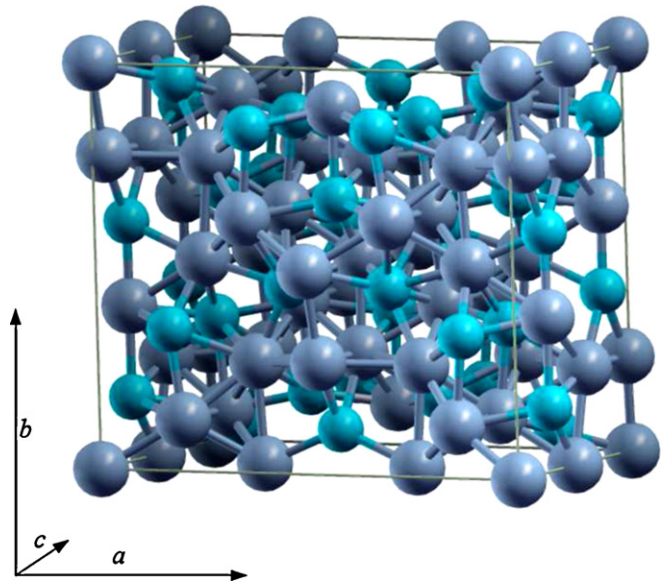

Fig. 5. Symbolic representation of ε-Ni_3Si_2.

Table 4
Symmetry and frequencies (in cm^{-1}) of modes α-$NiSi_2$ in Γ. We report all experimental data associated by Zhao at α.

Theo.	295 (T_{1u}, IR)		316 (T_{2g}, R)	
Expt. [25]	232	297	320	402

In the literature, Zhao has measured its Raman shifts [25]. We have thus calculated vibrational frequencies (ESPRESSO [26], DFTP calculations), and reported in the Table 4 frequencies in Γ. Although we can not compute Raman spectra due to the metallic nature of the phase, we can compare Γ frequencies. There are 6 non-zero frequencies, grouped in two irreducible representations: T_{2g}, and T_{1u}. The first one can be Raman active and the second one infrared active. We report also frequencies of NiSi-MnP phase at the Γ point in the Table 5 calculated in an other way [7]. The group theory can associate vibrational modes in accordance with the irreducible representations (D_{2h}^{16} point group): $A_{g,u}$ and $B_{g,u}$. Only "gerade" modes are Raman active, whereas the "ungerade" modes are infrared active.

Our simulations reproduce with accuracy all experimental Raman shifts [25]. We can note that only one mode can be associated to $NiSi_2$ (320 cm^{-1}), other peaks are those of MnP-NiSi.

3.8. *NiSi-L1$_0$, NiSi$_3$-L1$_2$, -D0$_3$, and -D0$_{22}$, and Si-A1*

For information, we have investigated three $NiSi_3$ structures ($L1_2$, $D0_3$, and $D0_{22}$) and NiSi-$L1_0$ (see Table 1). For all these structures, formation energies are found positive.

Concerning Si-A1 (fcc) structure, our results and those of Tokunaga [2] are in very good agreement.

Table 5
Symmetry and frequencies of o-NiSi in Γ. We have underlined the correspondence with experimental measurements.

A_g	150	194	214	286	330	351
A_u	0	163	214	271	285	374
B_g	193	219	251	312	330	397
B_u	0	0	182	290	316	377
Expt. [25]	195	214	258	294	332	362

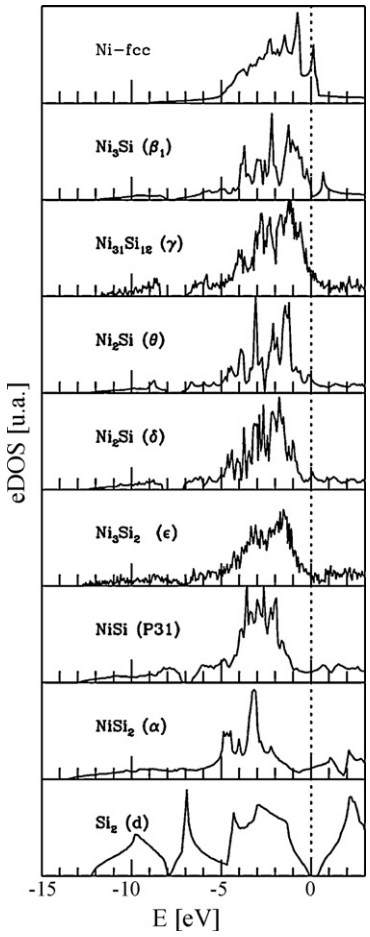

Fig. 6. Electronic density of states of the experimental Ni–Si alloys. Zero energy corresponds to the position of the Fermi level.

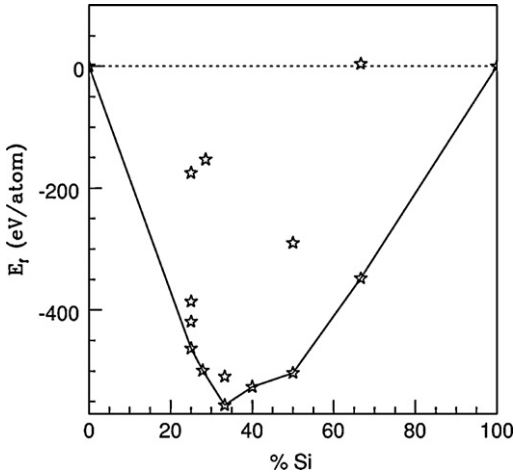

Fig. 7. Formation energies as a function of composition in at.% silicon.

4. Electronic properties and conclusion

We have calculated and plotted Fig. 6 electronic density of states of experimental systems. The Fermi levels have been aligned to facilitate the comparison. The Fermi level position is considered as very important for the stability of the intermetallic compounds.

We note that Fermi energies are close to a local minimum, except for γ. However, lower $N(E_f)$ (per atom) are not associated to

the more stable systems. Ni_3Si-$L1_2$ and Ni_3Si_2-ε have lower density of states (around 0.15 states/eV/atom), while the more stable system has a higher $N(E_f)$ (δ, with 0.46 states/eV/atom).

We provide a projected *e*DOS analysis on *s*, *p* and *d* orbitals. At low energy, for all the density of states, one finds that the *s* states from silicon are separated from the *d* states by an energy gap. At the Fermi level, *d* states of Ni are hybridized with the *p* states of silicon, and they form the bonds. One can note also that Ni–Si alloys are all non-ferromagnetic systems, in agreement with experimental findings [27].

In conclusion, in this work we have performed a systematic study by means of the DFT of lattice parameters and formation energies of nickel-silicides ordered alloys. As we have shown, for main experimental systems, our simulations reproduce lattice parameters and formation energies with a good accuracy. Fig. 7, we have summarized results on formation energies of all phases at 0 K. The importance of this binary system in many fields of application suggests that this new set of data should be used in assessments containing Ni–Si binary systems.

Acknowledgments

This work was granted access to the HPC resources of CALMIP (CICT Toulouse, France) under the allocation 2010-p0749.

References

[1] M. Lindholm, B. Sundman, Metall. Trans. A 26A (1996) 2897.
[2] T. Tokunaga, K. Nishio, H. Ohtani, M. Hasebe, Comput. Coupling Phase Diagrams Thermochem. 27 (2003) 161.
[3] T.B. Massalski, P.R. Subramanian, H. Okamoto, L. Kacprzak, Binary Alloy Phase Diagrams, second ed., ASM International, Materials Park, OH, 1990.
[4] G. Kresse, J. Hafner, Phys. Rev. B 47 (1993) 558;
G. Kresse, J. Hafner, Phys. Rev. B 49 (1994) 14251;
G. Kresse, J. Furthmüller, Phys. Rev. B 54 (1996) 11169;
G. Kresse, J. Furthmüller, Comput. Mater. Sci. 6 (1996) 15.
[5] J.P. Perdew, K. Burke, M. Ernzerhof, Phys. Rev. Lett. 77 (1996) 3865;
J.P. Perdew, K. Burke, M. Ernzerhof, Phys. Rev. Lett. 78 (1997) 1396.
[6] Z. Kresse, J. Joubert, Phys. Rev. B 59 (1999) 1758.
[7] D. Connétable, O. Thomas, Phys. Rev. B 79 (2009) 094101.
[8] C. Kittel, Introduction to Solid State Physics, Wiley, New York, 1996.
[9] E.H. Megchiche, S. Pérusin, J.C. Barthelat, C. Mijoule, Phys. Rev. B 74 (2006) 064111.
[10] Y. Oya, T. Suzuki, Zeitschrigt für Metallkunde 74 (1983) 21.
[11] S. Leballi, S. Hamar-Thibault, Zeitschrigt für Metallkunde 75 (1984) 764.
[12] R.P. Ram, S. Bhan, Zeitschrigt für Metallkunde 66 (1975) 521.
[13] S. Bhan, H. Kudielka, Zeitschrigt für Metallkunde 69 (1978) 333.
[14] Y. Song, S. Jin, Appl. Phys. Lett. 90 (2007) 173122.
[15] K. Frank, K. Schubert, Acta Crystallogr. B27 (1971) 916.
[16] W. Oelson, H. Samson-Himmelstjerna, Mitt. Kaiser-Wilhelm Inst. Eisenforch. Düsseldorf 18 (1936) 131.
[17] F. Bosselet, J.C. Viala, C. Colin, B.F. Mentzen, J. Bouix, Mater. Sci. Eng. A 167 (1993) 147.
[18] K. Toman, Acta Crystallogr. 5 (1952) 329.
[19] J.Y. Dai, D. Mangelinck, S.K. Lahiri, Appl. Phys. Lett. 75 (1999) 2214.
[20] D.F. Wilson, O.B. Cavin, Scr. Metall. Mater. 26 (1992) 85.
[21] F.M. d'Heurle, C.S. Petersson, J.E. Baglin, S.J. La Placa, C.X. Wong, J. Appl. Phys. 55 (1984) 4208.
[22] H. Föll, P.S. Ho, K.N. Btu, Philos. Mag. A 45 (1982) 31.
[23] K.W. Richter, K. Chandrasekaran, H. Ipser, Intermetallics 12 (2004) 545.
[24] G. Pilström, Acta Chem. Scand. 15 (1961) 893.
[25] F.F. Zhao, S.Y. Chen, Z.X. Shen, X.S. Gao, J.Z. Zheng, A.K. See, L.H. Chan, J. Vac. Sci. Technol. B 21 (2003) 862.
[26] P. Giannozzi, S. Baroni, N. Bonini, M. Calandra, R. Car, C. Cavazzoni, D. Ceresoli, G.L. Chiarotti, M. Cococcioni, I. Dabo, A. Dal Corso, S. Fabris, G. Fratesi, S. de Gironcoli, R. Gebauer, U. Gerstmann, C. Gougoussis, A. Kokalj, M. Lazzeri, L. Martin-Samos, N. Marzari, F. Mauri, R. Mazzarello, S. Paolini, A. Pasquarello, L. Paulatto, C. Sbraccia, S. Scandolo, G. Sclauzero, A.P. Seitsonen, A. Smogunov, P. Umari, R.M. Wentzcovitch, J. Phys.:Condens. Matter 21 (2009) 395502, http://arxiv.org/abs/0906.2569.
[27] B. Meyer, U. Gottlieb, O. Laborde, H. Yang, J.C. Lasjaunia, A. Sulpice, R. Madar, J. Alloys Compd. 262–263 (1997) 235.